ELSEVIER

Biophysical Chemistry 95 (2002) 253–272

Biophysical Chemistry

www.elsevier.com/locate/bpc

Structural basis for the unusual properties of 2′,5′ nucleic acids and their complexes with RNA and DNA

B.J. Premraj, S. Raja, N. Yathindra*

Department of Crystallography and Biophysics, University of Madras, Guindy Campus, Chennai 600 025, India

Received 14 March 2001; accepted 6 June 2001

Abstract

To provide insights into the unusual properties of 2′,5′ nucleic acids (*iso* nucleic acids), that includes their rejection by Nature as information molecules, modeling studies have been carried out to examine if they indeed possess the stereochemical ability to form helical duplexes and triplexes, just as their 3′,5′ linked constitutional isomers. The results show that the formation of helical duplexes with 2′,5′ linkages demands a mandatory displacement of the Watson and Crick base pairs from the helical axis, as a direct consequence of the lateral shift of the sugar–phosphate backbone from the periphery towards the interior of the helix. Thus, both duplexes and triplexes formed with a 2′,5′-sugar–phosphate backbone possess this intrinsic trait, manifested normally only in A type duplexes of DNA and RNA. It was found that only a 10-fold symmetric parallel triplex with isomorphous T·AT triplets is stereochemically favorable for *iso*DNA with '*extended*' nucleotide repeats, unlike the 12-fold symmetric triplex favored by DNA. The wider nature of a 12-fold triplex, concomitant with mandatory slide requirement for helix formation in *iso*DNA, demands even larger displacement, especially with '*extended*' nucleotide structural repeats, thereby violating symmetry. However, a symmetric triplex possessing higher twist, can be naturally formed for *iso*DNA with a '*compact*' nucleotide repeat. Two nanosecond molecular dynamics simulation of a 2′,5′-B DNA duplex, formed with an intrinsic base pair displacement of −3.3 Å, does not seem to favor a total transition to a typical A type duplex, although enhanced slide, X-displacement, decrease in helical rise and narrowing of the major groove during simulation seem to indicate a trend. Modeling of the interaction between the chimeric *iso*DNA·RNA duplex and *E. coli* RNase H has provided a structural basis for the inhibitory action of the enzyme. Interaction of residues Gln 80, Trp 81, Asn 16 and Lys 99, of *E. coli* RNase H with DNA of the DNA·RNA hybrid, are lost when the DNA backbone is replaced by *iso*DNA. Based on modeling and experimental observations, it is argued that 2′,5′ nucleic acids possess restricted conformational flexibility for helical polymorphism. The inability of *iso*DNA to favor the biologically relevant B form duplex and the associated topological inadequacies related to nucleic acid compaction and interactions with regulatory proteins may be some of the factors that might have led to the rejection of 2′,5′ links.

Keywords: *iso*DNA duplexes and triplexes; Molecular dynamics; Nucleic acids evolution; *E. coli* RNase H–substrate interaction; *E. coli* RNase H inhibitor interaction; *iso*DNA·RNA duplex

*Corresponding author. Tel.: +91-44-230-0122; fax: +91-44-235-2494.
E-mail address: ny@vsnl.com (N. Yathindra).

0301-4622/02/$ - see front matter
PII: S0301-4622(02)00040-6

1. Introduction

It is abundantly clear that the paradigm molecular recognition interaction manifested in the Watson and Crick base pairing scheme supports a wide variety of chemical scaffolds, including even those without the sugar–phosphate moiety. Surprisingly, the stability of some of these duplexes has been shown to be even higher by 1–5 °C per base pair compared to DNA and RNA duplexes. This has led to the proposition that optimization, rather than maximization of duplex stability, was perhaps the selection criterion adopted by nature to settle the backbone chemistry of informational molecules [1]. It is recognized that the ability to form a duplex, the structural vehicle for information storage and transmission, represents the mandatory first step for any molecule to serve as an informational molecule [2]. While it is known that this can be satisfied by a variety of backbone scaffolds [1–8], it is pertinent to ask to what extent the geometry and topological features of some of these duplexes become relevant, especially in view of the observation that many of these scaffolds exhibit structural features nowhere close to the helical duplexes described for DNA and RNA. This brings into focus the question whether there was also an additional selection criterion related to the optimization of topological and geometrical features for the selection of the backbone chemistry of the informational molecule. This argument is not unreasonable in view of the known stringent requirements of DNA to be able to undergo several orders of compaction and flexibility required for interaction with regulatory proteins. It is, therefore, to be expected that only certain geometries for the double helix, such as B DNA, can alone facilitate this. Thus, optimization of both duplex stability and helix topology must have been the guiding factors for settling the chemical etiology of nucleic acids. In this context, it is intriguing to see why nucleic acids with 2′,5′ linkages (Fig. 1), the constitutional isomer and also the closest chemical mimetic of the naturally occurring 3′,5′ linked nucleic acids, were not used by nature as informational molecule. Surprisingly, it was believed for long that they do not support Watson and Crick associations, and this impediment was considered to be the sole factor for their rejection [9–11]. However, in recent years, it has been conclusively

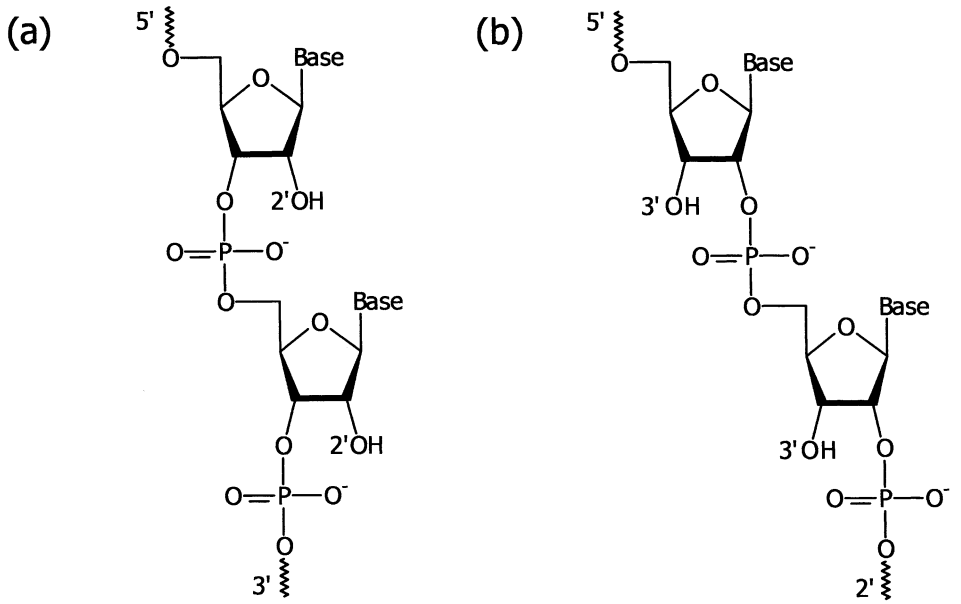

Fig. 1. Schematic representation of (a) 3′,5′ linked and (b) 2′,5′ linked nucleic acids (*iso* nucleic acids).

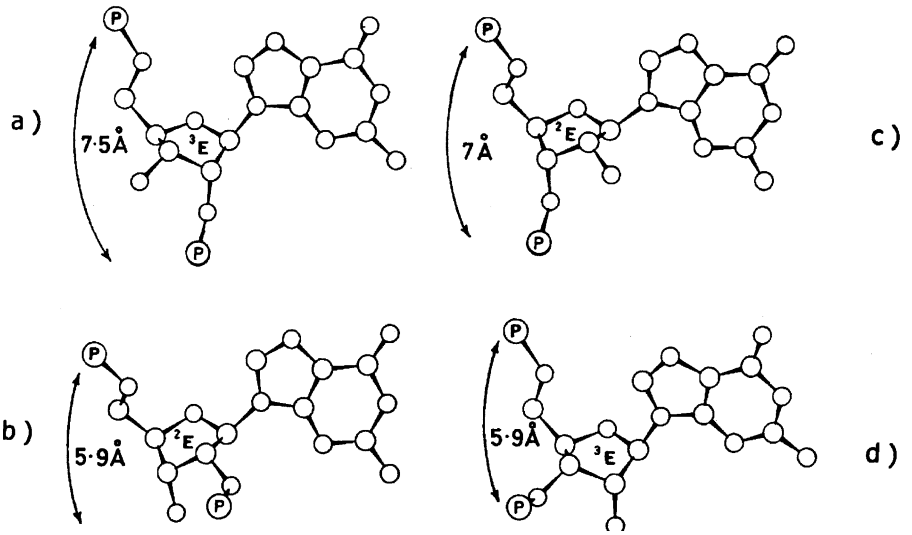

Fig. 2. Preferred conformations for the repeating structural units in 2′,5′ (a, b) and 3′,5′ (c, d) nucleic acids for the commonly found C3′*endo* and C2′*endo* sugar puckers. Equatorial linkages (C3′–O3′/C2′–O2′) lead to the *compact* form (P…P=5.9 Å), while axial linkages lead to the *extended* form (P…P=7 Å). An inverse relationship between nucleotide shapes and linkage type is clearly discernible.

established [12–20] that the sugar–phosphate backbone scaffold, even with 2′,5′ linkages, supports Watson and Crick paired duplex structures, suggesting that factors other than the mechanistic aspect of duplex formation, per se, may be responsible for nature's rejection of 2′,5′ links. It is also known that 2′,5′ isomers even complex with the 3′,5′ strands to form duplexes and triplexes, and they exhibit unusual properties [19–26]. Some of these include the selective preference of 2′,5′ DNA/2′,5′ RNA (*iso*DNA/*iso*RNA) for complexation with RNA as opposed with DNA, low T_n for the helical complexes, and an usually high stability for *iso*DNA·RNA chimeric complex concomitant with the latter's strong resistance to *E. coli* RNase H cleavage [20,25–27]. An attempt has been made here, from stereochemical investigations, to provide a structural basis for some of these and to offer clues for nature's rejection of 2′,5′ isomers in favor of 2′,5′ isomers.

2. Methods

Our earlier studies have clearly brought out the fundamental differences that exist in the shapes of the repeating nucleotides in 2′,5′ and 3′,5′ nucleic acids [16,17]. These have led to the description of the nucleotide structural repeat in terms of compact and extended conformation in order to unify the description and generation of nucleic acid helices independent of the type of linkage and without recourse to sugar pucker-based semantics (Fig. 2). These have greatly facilitated modeling of duplex and triplex helical complexes, comprising not only exclusively 2′,5′ linked strands, but also chimers formed by the complexation of 2′,5′ and 3′,5′ strands. These concepts are used here to build helical structures of 2′,5′ isomers as well as their complexes with 3′,5′ isomers. Wherever necessary, they are subjected to stereochemical refinement using the Linked Atom Least Squares method (LALS) [28]. Such procedures are extensively employed to arrive at structural models from diffraction patterns of nucleic acids and polynucleotides [29–31]. Molecular dynamics simulations were carried out using the force field of Cornell et al. [32] embodied in the Sander module of AMBER 4.1 suite [33], taking into account explicit solvent counterions, with complete realization of the long range electrostatics using the Particle

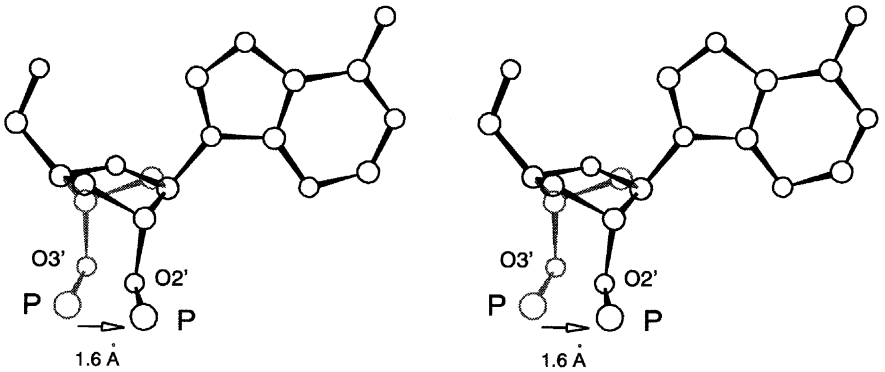

Fig. 3. Stereoplot of the superposition of extended nucleotide repeats in 3′,5′ (gray) and 2′,5′ nucleic acids (black). Shift of phosphate location leads to shift in base pairs necessitating slide and *X*-displacement for base pairs in 2′,5′ linked nucleic acids (see text).

Mesh Ewald (PME) method [34]. All the protocols conforming to state-of-the art methodology have been followed. A database for the nucleic acid building block with 2′,5′ links has been created. Partial charges and force field atom types were appropriately modified to obtain proper geometry and stereochemistry at 2′,5′ sugar–phosphate linkage. Water and counterions were added to the DNA using the LEaP module. The system was initially subjected to equilibration, followed by a production run using standard procedures [35]. The results were analyzed using the various modules available with AMBER 4.1, the Dials and Windows interface to Curves [36] and a recent version of Curves (Ver. 5.1) [37]. Molecular dynamics simulations were either run on an SGI Octane workstation or Pentium III PC on a RedHat linux 6.2 platform.

Using the 11-fold model $DNA^{C2'endo}$·$RNA^{C3'endo}$ hybrid duplex obtained from fiber diffraction data as the initial model [38], $DNA^{O4'endo}$·RNA, $DNA^{C3'endo}$·RNA and *iso*-DNA·RNA hybrid duplex models have been obtained through constrained energy minimization using the AMBER 4.1 suite [33]. The docking of the hybrid duplexes with *E. coli* RNase H and the subsequent interaction studies were carried out using the graphics interface of Insight II [39] on an Octane SGI workstation.

3. Results and discussion

3.1. Molecular dynamics of 2′,5′ B DNA duplex

Our earlier investigations have revealed that a 2′,5′ B DNA helical duplex structure is not stereochemically feasible without a mandatory slide of at least −2.2 Å and a concomitant *X*-displacement (*X*-disp) of −3.3 Å for the base pairs [17] (values of slide and *X*-disp calculated using Curves are higher by −0.5 and −0.8 Å, respectively, compared to values of slide of −1.7 Å and *X*-disp = −2.5 Å obtained using other nucleic acid analysis programs). This is because of the lateral shift of the sugar–phosphate chain link from the O3′ to the O2′ atom of the sugar (Fig. 3) to facilitate 2′,5′ linkage, which leads to natural sliding of the base pairs towards the interior of the helix. This results in reduced intra-strand adjacent base overlap compared to B DNA and this might be one of the reasons for the observed lower T_m for the *iso*DNA duplex fragments [13,14,25]. Linkage change also causes the phosphates to move away such that the major groove expands concomitant with compression in minor groove. Their magnitudes correspond to 14 and 4.7 Å (5.8 Å subtracted to account for the van der Waal's radii of the phosphate groups), respectively, compared to the values of 11.7 and 5.9 Å found for ideal B DNA. A typical homopolymer *iso*DNA duplex

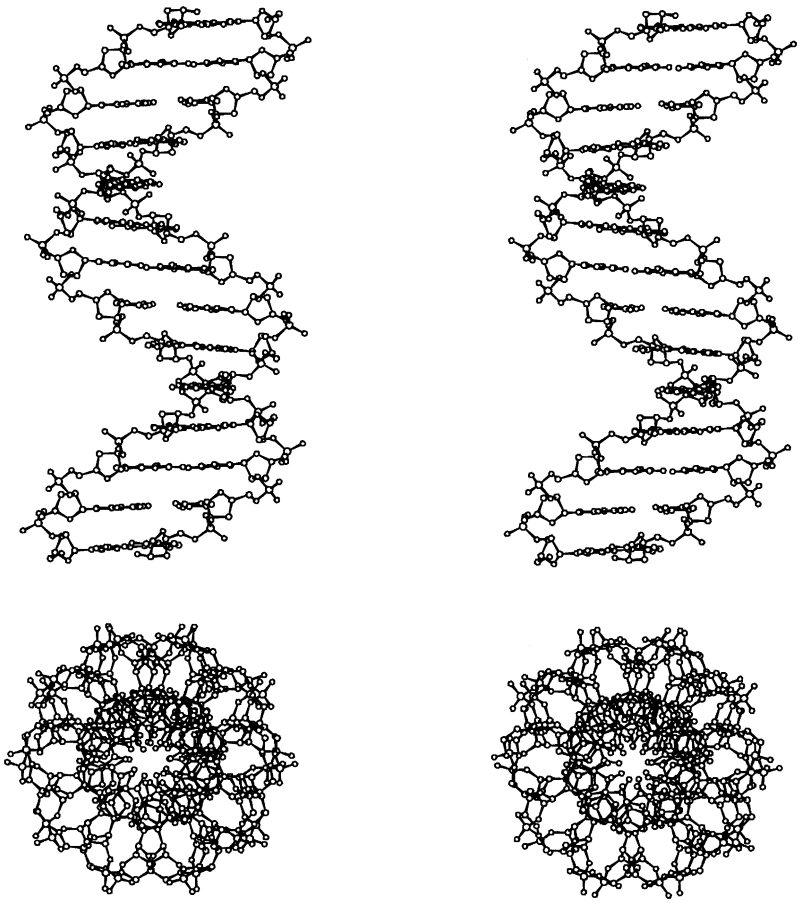

Fig. 4. Stereoplot of LALS generated 2′,5′ B DNA duplex viewed perpendicular (top) and parallel (bottom) to the helix axis. Least values of slide (−1.7 Å) and *X*-displacement (−2.5 Å) needed for stereochemical feasibility are used. Duplex is made up of extended (P…P=7.2 Å) C3′*endo* nucleotide repeats with a (g^-, g^-) phosphodiester conformation. Note the central hole down the helix axis, a trait of the A-type helix and the base pairs perpendicular to helix axis, a trait of the B-type duplex.

comprising G…C base pairs and formed with *extended* C3′*endo* nucleotide repeats is shown in Fig. 4. Since the structure possesses the intrinsic traits of an A-type duplex, namely, slide (−2.2 Å) and *X*-displacement (−3.3 Å), it is felt that this may correspond to an intermediate conformation of A and B type duplexes, and the structure may perhaps favor an A type duplex by seeking optimal values for slide and displacement with concomitant sugar repuckering. This argument is supported by the observation of an A type duplex for an *iso*DNA fragment from NMR studies [18]. In order to examine the possibility of a B⇒A transition of *iso*B DNA and to obtain a detailed insight into the nature of conformational flexibility towards helical polymorphism of 2′,5′ linked nucleic acids, a 2-ns molecular dynamics simulation (MDS1) has been carried out on *iso*B DNA. A 2-ns MD simulation in the presence of 1 M NaCl (MDS2) was also carried out since it has been shown that high salt stabilizes Watson and Crick association in *iso* nucleic acids [13,19,23,25].

3.1.1. Analysis of the MD trajectory and structural features

Fig. 5 shows the nature of variation of slide and *X*-displacement (*X*-disp) during the 2-ns MD sim-

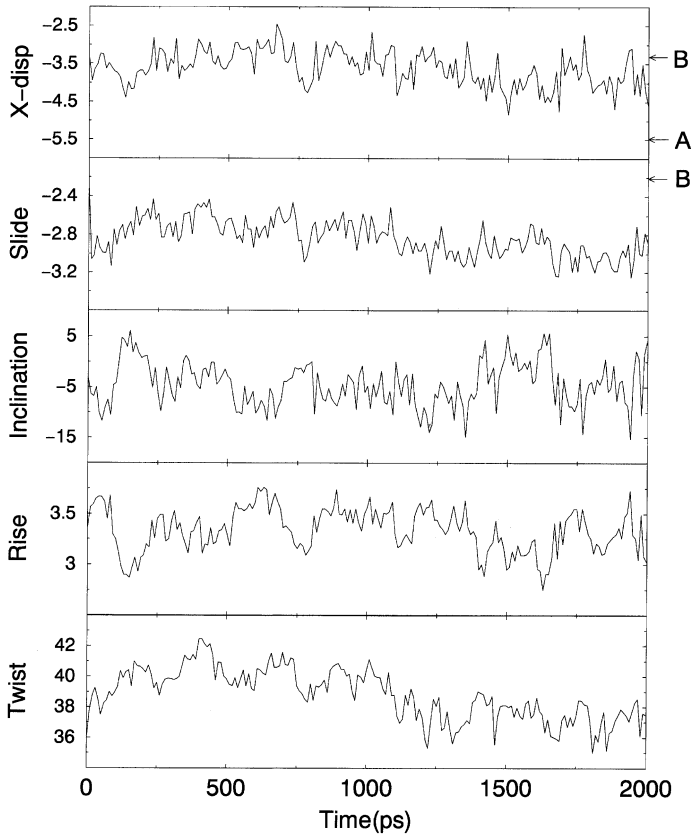

Fig. 5. Variation of helical and base-pair parameters of the central decamer duplex taken at 10-ps intervals over the 2-ns MD simulation. A large variation in slide and *X*-disp is evident (values of slide and *X*-disp calculated using Curves are higher by −0.5 and −0.8 Å, respectively, compared to those obtained using other nucleic acid analysis programs). A preference for higher twist over the first nanosecond and stabilization of the twist values between 35° and 38° in the final 750-ps. Also note the preference for low values of rise over a short interval of time. A and B represent values corresponding to ideal *iso* A DNA and *iso* B DNA structures, respectively.

ulation (MDS1). Both of these exhibit large variation, with slide varying from −2.4 to −3.2 Å, and displacement from −2.5 to −4.5 Å. These values, especially the higher ones, however, do not persist for a long enough duration of time to suggest a clear B⇒A transition. Also, they are not accompanied by base pair inclination (with respect to the helical axis) and repuckering of the sugar to affect a *compact* C2′*endo* structural repeat, which is required to facilitate a complete B⇒A transition.

The helical twist shows a preference towards higher values (40–43°) during the initial 1000 ps, and this is accompanied by lower values of slide (−2.6 Å), suggesting a more tightly wound duplex structure. During the final 750 ps, the helical twists follow a downward trend and finally stabilize at values between 36° and 38°, corresponding to a 10-fold *iso*B DNA-like duplex with slightly larger values (−3.0 Å) of slide. A low helical rise (2.8 Å) was observed at approximately 150 and 1500 ps, and although indicative of a possible trend towards an A-type helix, the inclination angles (5°) are not large enough. Moreover, these trends last only for short intervals of time.

Helix grooves show marked variation, with the major groove width exhibiting larger variations (6–16 Å) than minor groove width (4–6 Å) (Fig.

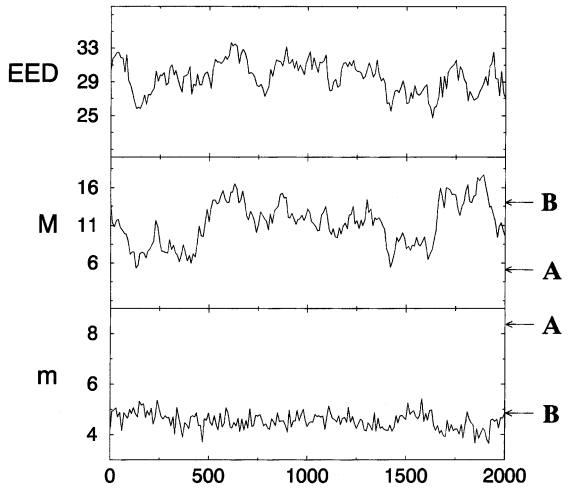

Fig. 6. Variation of end-to-end distance of the central decamer duplex, major (M) and minor (m) groove widths over the 2-ns MD simulation (MDS1) of *iso* B DNA. Narrowing of the major groove at approximately 260–400 and 1400–1625 ps concomitant with a reduction in end-to-end distance, indicates the traits of the A-form duplex. A and B represent values corresponding to ideal *iso* A DNA and *iso* B DNA structures, respectively.

6). Narrowing of the major groove, concomitant with a reduction in the end-to-end distance of duplex (see Fig. 6), occurs during 260–400 and 1400–1625 ps, indicating a possible trend towards an A-type duplex, though there is no concerted increase in the inclination angle of the base pairs, decrease in rise or repuckering of the sugar pucker from C3′*endo* to C2′*endo* conformation to provide a *compact* structural repeat. Recent NMR studies have confirmed that it is the *compact* C2′*endo* nucleotide repeat that forms structural repeats in A-type duplexes for *iso* nucleic acids [40]. Superposition of the snapshots of the duplexes at regular intervals between 1400 and 1625 ps is shown in Fig. 7.

Though variations in groove widths, helical and base pair parameters seemingly indicate a trend towards A-type duplex, no definitive assertions may be made to invoke a total B⇒A transition as these variations do not last for sufficiently long duration of time.

Analysis of the trajectory shows that the structural repeat retains the *extended* nucleotide conformation throughout the simulation with the sugar puckers remaining in the C3′*endo* domain and the backbone torsions ε-(C2′–O2′), β(C5′–O5′) and

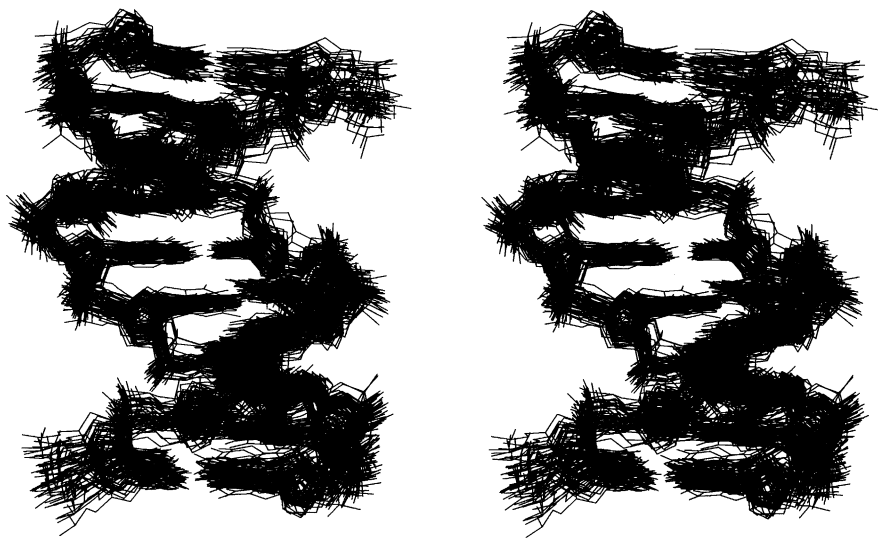

Fig. 7. Superposition of the central decamer duplex of 44 structures over the time period 1400–1625 ps (MDS1). Large *X*-displacement, narrow major groove width and reduced end-to-end distance, which are traits of the A-form duplex, can be seen although the repeating nucleotide retains the *extended* C3′*endo* nucleotide conformation.

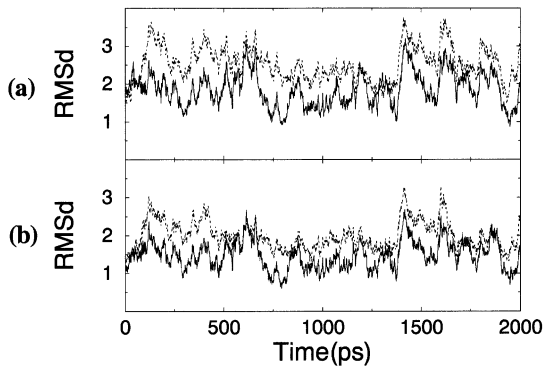

Fig. 8. RMSd vs. time (ps) plot for (a) the central decamer duplex and (b) 14-mer duplex with respect to the average structure (bold lines) and starting structure (dotted lines), for structures taken at 1-ps intervals over the 2-ns MD trajectory (MDS1).

γ(C4′–C5′) torsions largely favoring the preferred *gauche*$^-$, *trans* and *gauche*$^+$ conformational domains, respectively. The phosphodiester P–O2′ (ζ) and P–O5′ (α) conformations remain in the (g^-, g^+) domain throughout the simulation. In a few cases, it goes over to (g^-, g^+) conformation when α switches to *gauche*$^+$ with concomitant switch in γ from *gauche*$^+$ to *trans*, conforming to the well-known long range correlation between α and γ observed in DNA and RNA duplexes [41–43].

The root mean square deviation (RMSd) for the central decamer of all the structures taken at 1-ps intervals over the 2-ns simulation is between 0.6 and 2.7 Å and between 1.9 and 3.2 Å from the average and starting structures, respectively (Fig. 8). Higher RMSd is due to drastic variation in slide and *X*-disp, as well as narrowing of major groove widths during the course of the simulation. Average duplex structure over the 2-ns MD simulation (MDS1) is shown in Fig. 9. The large slide (−2.8 Å) and *X*-displacement (−4.2 Å) (traits of an A-form duplex) and stacking interaction are similar to that found in A DNA, while tiltless bases are reminiscent of a B-form duplex. The structure represents more of an intermediate duplex between A and B DNA forms, similar to the average structure observed in the MD simulation of $d(C_4G_4)_2$ [44], which has A-type base stacking, but an *extended* C2′*endo* nucleotide repeat.

Analysis of the 2-ns MD simulation in 1 M NaCl shows that the 2′,5′ B DNA duplex is comparatively more stable. Variation in slide and *X*-disp is comparatively less, although there is a tendency towards higher values of slide compared to the minimum value of −2.2 Å required for the formation of 2′,5′ B DNA. Minor groove widths fall within the broad range observed earlier, while slight narrowing of major groove widths (11–12 Å) is also seen. RMSds of the central decamer, taken at 1-ps intervals over the 2-ns MD simulation, is between 0.6 and 2.0 Å and between 1.3 and 2.9 Å, from the average and starting structure, respectively. These are much less compared to those observed in the absence of high salt (MDS1), indicating higher stability.

3.1.2. Hydration

Hydration pattern around the *iso* B DNA duplex shows that, on average, anionic oxygen atoms are individually hydrated by three waters along the vertices of a trigonal pyramid due to *extended* nucleotide repeat (P…P≈7.2 Å). Hydration sites for guanine are seen at approximately N3 and N2 (minor groove side), O6 and N7 (major groove side). For cytosine, hydration sites are observed at approximately O2 and N4. These are similar to those observed for B DNA [45,46].

Results from both the MD simulation (MDS1 and MDS2) on 2′,5′ B DNA confirm the mandatory requirement of slide cum *X*-disp. Although a tendency for a B⇒A transition is manifested through the narrowing of the major groove, an increase in slide and *X*-disp, and a decrease in helical rise during the course of the simulation, other concerted changes, such as base pair inclination and flipping of sugar pucker from C3′*endo* to C2′*endo* to provide a *compact* form for the nucleotide repeat required to invoke a total transition to A form are not evident. Thus, the average structure from the NM simulations of 2′,5′ B DNA retains the qualitative features of the initial model but with enhanced values for slide and *X*-displacement, features of the A form duplex.

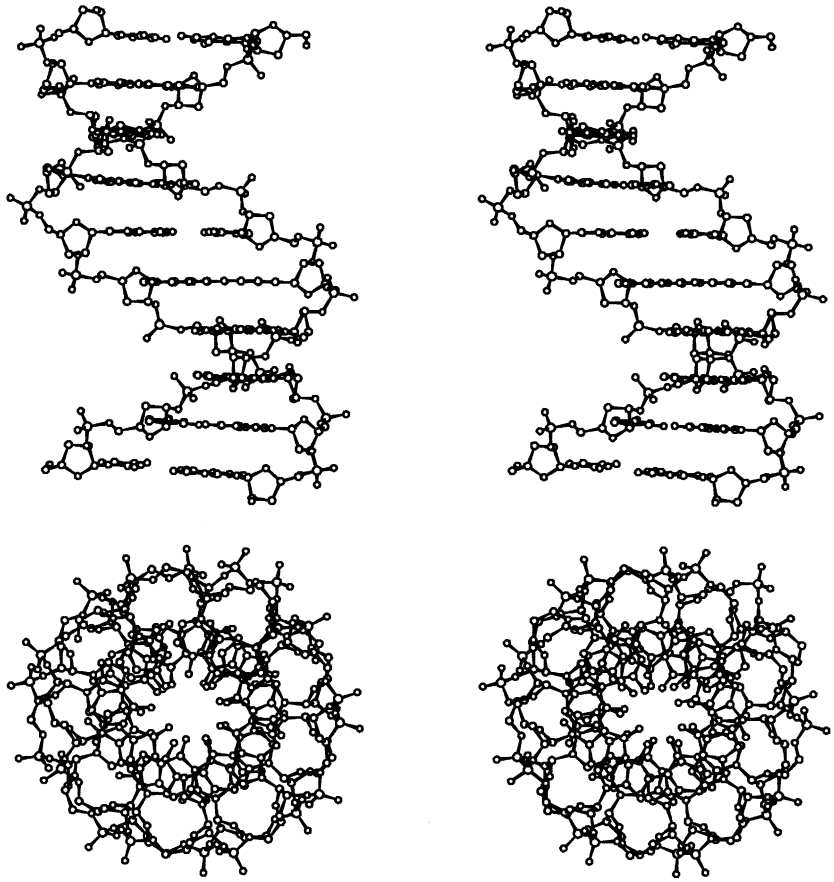

Fig. 9. Stereoview of the average structure for the central decamer duplex over the 2-ns trajectory (MDS1) viewed perpendicular (top) and parallel (bottom) to the helix axis. The structure represents more of an intermediate between the A and B type helix. Note the large slide (−2.83 Å) and *X*-displacement (−4.2 Å) (traits of the A-form duplex) and stacking interaction similar to that found in A DNA. Tiltless bases and extended nucleotide conformation are reminiscent of the B-form duplex.

3.1.3. Structural characterization of 2′,5′ DNA triplexes

It is well known that Watson and Crick DNA and RNA duplexes support a third strand along their major groove, stabilized by Hoogsteen or reverse Hoogsteen base pairs [47]. That this idea has developed into an important strategy for gene regulation is well documented [48,49]. A symmetric structural model for the 12-fold DNA triplex [50] comprising T·AT base triads (Fig. 10) and with *extended* C2′*endo* nucleotide repeats (P…P= 6.8 Å) for all the chains has been proposed, consistent with a number of experimental evidences [51,52] and MD simulation studies [53]. Attempts to generate such a symmetric 2′,5′ DNA triplex with T·AT triplets (see Fig. 10) using the linked atom least squares (LALS) approach and by using *extended* C3′*endo* nucleotide structural repeats (P…P=7.2 Å) (see Fig. 2) show that only a 10-fold triplex ($t=36°$) is stereochemically feasible (Fig. 11). In this structure, Watson and Crick base pairs exhibit a displacement of −3.3 Å from the triple helical axis that is identical to that needed to form a stereochemically feasible *iso* B DNA duplex. Due to this, the duplex and the triplex helical axes of *iso*DNA coincide. In other words,

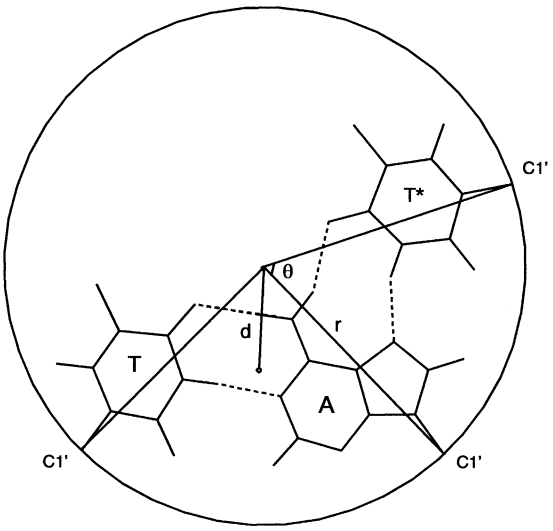

Fig. 10. Schematic diagram of T·AT base triplets showing the geometry and symmetry (47). The Hoogsteen A·T pair is related by a pseudorotational symmetry. The radius r of the helix with respect to C1′ atom is 7.3 Å, $\theta = 69.5°$ and X-disp $d = -2.5$ Å.

iso B DNA duplex is already pre-organized to facilitate the formation of a triplex due to displaced Watson and Crick pairs (X-disp $= -3.3$ Å) from the triple helical axis and expanded major groove width of 14 Å. It is to be recalled that both of these features occur subsequent to the formation of triplex in the case of DNA [50,53]. In other words, *iso* B DNA duplex need not undergo conformational changes to accommodate a third strand along its major groove unlike B DNA. The *iso*DNA triplex is stabilized by interactions between the methyl groups of one thymine and the adjacent thymine of the Hoogsteen strand (Fig. 12). The inherently less stable nature of 2′,5′ B DNA duplex, due to significantly lower intra-strand base stacking caused by the slide between adjacent base pairs, may be the reason for the observed single transition of 2′,5′ DNA triplex upon denaturation in contrast with the corresponding DNA triplex [54]. Reduced base stacking interaction in the *iso*DNA duplex, as implicated from modeling studies, derives support from thermodynamic studies, which show that the free energies of *iso*DNA duplexes are half as compared to those of the corresponding DNA duplexes [15]. Moreover, *iso*DNA triplexes are found to be thermodynamically less stable than the corresponding DNA triplexes due to lower enthalpy [54], which could be a consequence of reduced base stacking interaction in the duplex component of the former.

Attempts to generate a 12-fold ($t = 30°$) symmetric triplex for *iso*DNA with the *extended* C3′*endo* repeating nucleotide is found to be stereochemically unfeasible due to poor backbone geometry and severe steric overlap involving phosphate and adjacent sugar. This situation can be eased by increasing the value of slide (> -3.3 Å). This causes widening of the helix, resulting in a large diameter for the triplex, and which in turn, calls for higher displacement of the Watson and Crick base pairs. These changes result in violation of conditions (see Fig. 10) required for the formation of a symmetric triplex. Moreover, it is found that the displacement should be in a direction normal to the line joining the two C1′ atoms of the two thymines (of Watson and Hoogsteen strands) rather than X-displacement associated with the Watson and Crick pairs of the T·AT triplet. Such a triplex possesses a ribbon-like structure and necessarily results in a large void at the center. This also causes a dissimilar conformation for the adenine strand (highly extended with P…P > 8 Å) compared to the two thymine strands. In fact, such a triplex structure with a large void and comprising C2′*endo* nucleotide repeat has been reported for *iso*DNA triplex [55]. Our modeling studies further show that an 11-fold symmetric triplex for *iso*-DNA, without the need for such large displacement, is also found to be feasible with *compact* C2′*endo* nucleotide repeats (P…P = 6.1 Å) (Fig. 13). The structure has an X-displacement of -3.4 Å and a base pair inclination of 7.3°. It should be mentioned that it is not known if the 2′,5′ nucleic acid triplex will have the same helical parameters as DNA and RNA triplexes. It is possible that a symmetric 10-fold parallel symmetric triplex is favored by 2′,5′ DNA comprising T·AT triplets, in view of the ease with which it can be formed. In any case, it is clear from the present study that 2′,5′ links cannot form a triplex structure that is identical to that formed by DNA with 3′,5′ links.

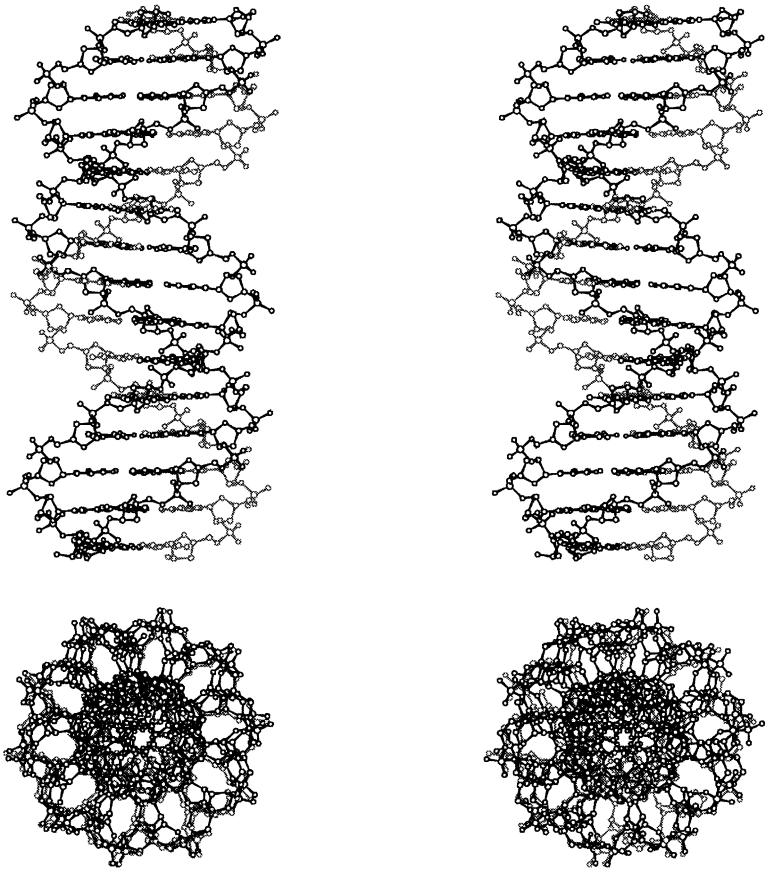

Fig. 11. Stereoplot of symmetric 10-fold parallel *iso*DNA triplex viewed perpendicular to the helical axis (top) and viewed parallel to helix axis (bottom), formed by T·AT triplets with *extended* C3′*endo* nucleotide repeat.

3.2. Structural basis for the inhibition of E. coli RNase H by isoDNA·RNA chimer

It is known that *iso*DNA forms a highly stable complex with RNA with a T_m value that is comparable to that of the DNA·RNA hybrid [9,23,25]. Interestingly, the complex is an inhibitor of *E. coli* RNase H and no structural rationale is forthcoming to explain this, perhaps due to lack of structural details of *iso*DNA·RNA hybrid. Knowing the distinct conformational difference that exists between the structural repeats in 2′,5′ and 3′,5′ nucleic acids (Fig. 2), it is anticipated that the structure of this chimer will exhibit features quite different from the DNA–RNA hybrid and these may offer clues for its role as an inhibitor. Therefore, the structure of the chimeric *iso*DNA·RNA duplex is modeled first, followed by its interaction with *E. coli* RNase H.

While modeling the structure of *iso*DNA·RNA duplex, it is assumed that RNA strand will impose its structure on the *iso*DNA strand. This is justifiable in view of the extensive experimental evidence indicating an exclusive preference for the A-type duplex by the DNA·RNA hybrid [56–64]. Hence, a *compact* nucleotide conformation is assumed to be the helical repeat in both *iso*DNA (comprising adenines) and RNA (comprising uridines) strands of the chimeric duplex. The phosphodiester linkage of the DNA strand in the 11-fold DNA·RNA hybrid duplex model [38] is modified to contain 2′,5′ linkages and the duplex

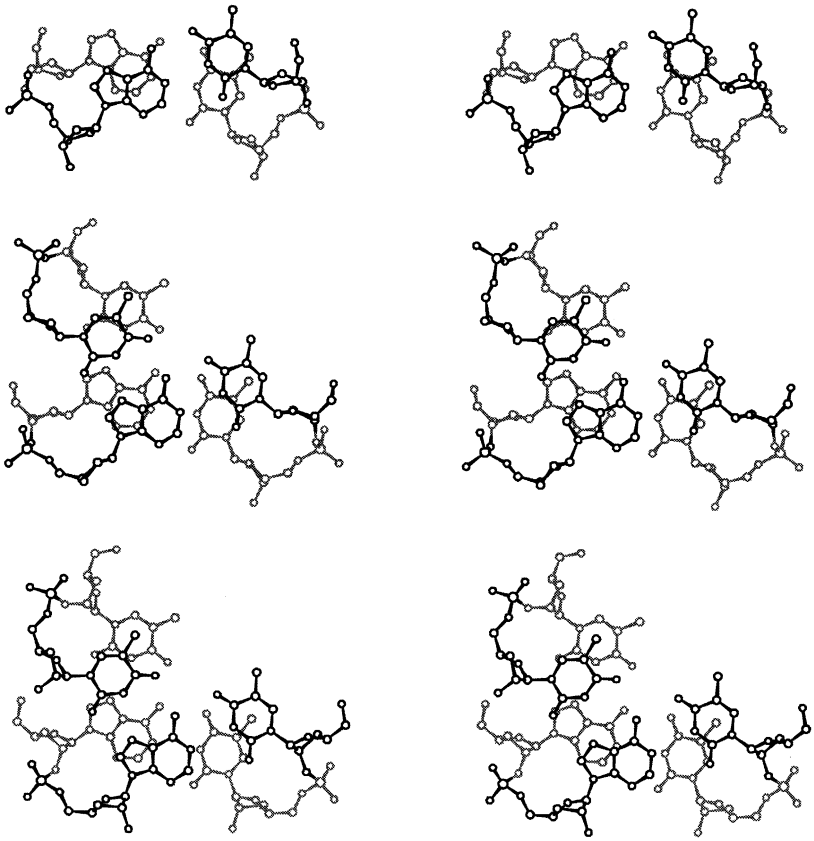

Fig. 12. Stereoplot of base stacking interaction in B DNA duplex (top), 12-fold DNA triplex (middle) and 10-fold *iso*DNA triplex (bottom) formed with *extended* structural repeat. Note the reduced stacking interaction in the *iso*DNA duplex. Also stabilization interactions involving the methyl groups of one thymine and the adjacent thymine of the Hoogsteen strand is evident.

is subjected to constrained energy minimization to obtain proper backbone stereochemistry. An A-type 11-fold duplex so generated for *iso*DNA·RNA is shown in Fig. 14. The *iso*DNA strand is characterized by the presence of *compact* C2′*endo* nucleotide repeats (P…P=6.0 Å) concomitant with a (t, g^-) phosphodiester conformation while the RNA strand possesses a *compact* C3′*endo* nucleotide repeats (P…P=5.9 Å) with a (g^-,g^-) phosphodiester conformation. A general pattern seen in *iso* nucleic acid duplexes, compared to DNA/RNAs, is that a switch from 3′,5′ to 2′,5′ linkage results in an expansion of the major groove and narrowing of the minor groove widths [16,17]. As a result, major and minor grooves of the chimeric duplex have widths of 8.2 and 9.1 Å, respectively, compared to the values of 6.3 and 10.8 Å found in the DNA·RNA hybrid [38] (Table 1). Incidentally, the minor groove width (9.1 Å) of the *iso*DNA·RNA duplex lies intermediate between the values seen for ideal A RNA (11.1 Å) and B DNA (5.7 Å) duplexes [65,66].

In order to elucidate structural features responsible for the inhibitory property of *iso*DNA·RNA, a 19-mer duplex is docked with the *E. coli* RNase H. Firstly an Mg^{2+} ion was placed at a distance of 2, 4.2, 4.5 and 4.9 Å to carbonyl oxygen of Asp 10, Glu 48, Asp 70, and Asp 134, respectively, as observed in the crystal structure of *E. coli* RNase H [67]. The hybrid was oriented along the line linking the Mg^{2+} binding site and the basic protrusion such that the scissile bond ($O3'–P_{11}$) is

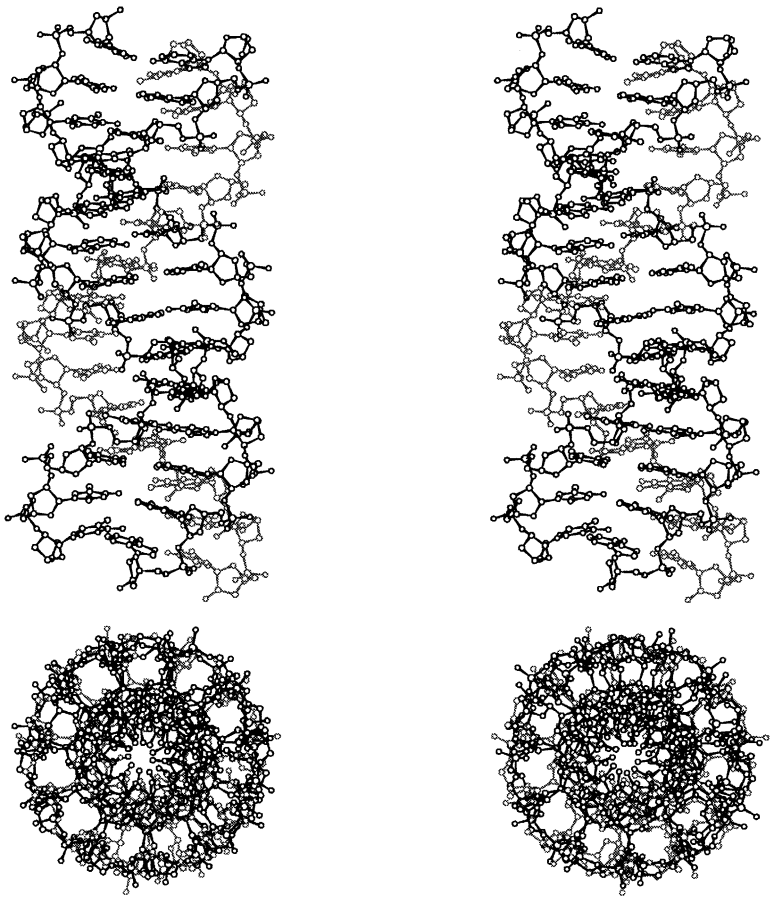

Fig. 13. Stereoplot of symmetric 11-fold parallel *iso*DNA triplex viewed perpendicular to the helix axis (top) and viewed down the helix axis (bottom), formed with T·AT triplets and *compact* C2′*endo* nucleotide repeat.

positioned close to the Mg^{2+} ($\sim$3.5 Å) [70]. This positioning and orientation of the chimeric duplex with RNase H is identical to the criteria suggested based on the crystal structure of *E. coli* RNase H [68] and also consistent with earlier models of a DNA·RNA×RNase H complex [64,69,71]. As a consequence, the RNA strand of both *iso*-DNA·RNA and DNA·RNA duplexes exhibit complete overlap, with the result that the proposed interactions of the residues Asp 94 (in the basic protrusion region), Cys 13 (Glycine rich loop), Gln 72 (α II helix), Lys 122, and Asn 44 with the RNA chain (Fig. 15) remain unaltered [63,67]. It may be pointed out that, although RNA duplex binds to *E. coli* RNase H, no cleavage occurs, thereby emphasizing that the non-cleaving DNA strand plays a role in interaction, complex formation and cleavage [71].

3.2.1. Interaction of E. coli RNase H with DNA$^{O4'endo}$ RNA hybrid

It has been proposed that an intermediate value for the minor groove width for the DNA·RNA hybrid duplex concomitant with O4′*endo* pucker for the sugar residues of the DNA strand is crucial for RNase H activity [64,72,73]. These observations are supported by recent studies, which incorporate constrained O4′*endo* sugars into the DNA strand of DNA·RNA hybrid [72,73]. However, no details concerning the interactions of the enzyme

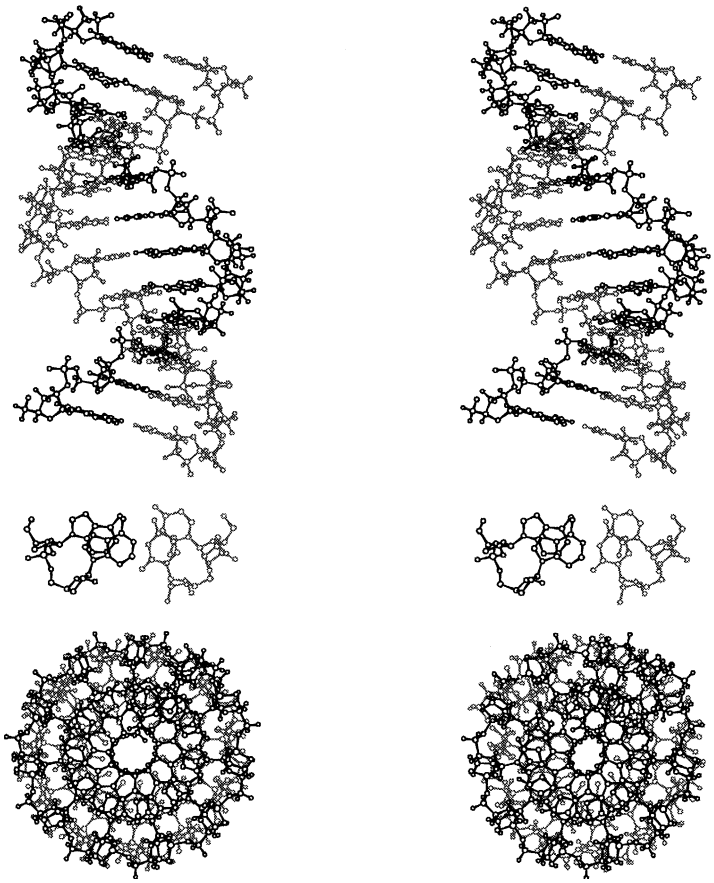

Fig. 14. Stereoplot of an 11-fold *iso*DNA·RNA, duplex (top) viewed perpendicular to the helix axis, (middle) adjacent base pair overlap to illustrate base stacking interaction and (bottom) *iso*DNA·RNA duplex viewed down the helix axis. The *iso*DNA strand has a *compact* C2′*endo*, nucleotide repeats and (t, g^-) phosphodiester conformation while the RNA chain has *compact* C3′*endo* nucleotide repeats and (g^-,g^-) phosphodiester conformation. Note the shift in the position of the phosphate group towards the interior of the helix in the *iso*DNA strand.

responsible for differentiating $DNA^{O4'endo}$ from $DNA^{C3'endo}$ in the DNA·RNA hybrid are available. It is needless to point out that knowledge of such information is important for the better understanding of the structural basis of *E. coli* RNase H action, since these would facilitate the design of oligonucleotides that will elicit RNase H action, important in the antisense approach of gene expression.

In order to delineate the role of O4′*endo* nucleotide repeat in the DNA chain of the DNA·RNA hybrid and its anticipated effect in increasing the minor groove width, thereby enhancing the specific enzyme–substrate interactions, we have modeled an 11-fold DNA·RNA hybrid duplex, as well as its interaction with *E. coli* RNase H. Modeling studies show that the presence of O4′*endo* sugars in the DNA strand instead of C3′*endo* sugars results in a decrease in the minor groove width by approximately 0.9 Å (Table 1). However, more importantly, the occurrence of an O4′*endo* sugar pucker in the DNA chain renders the anionic oxygen atoms of the phosphate to orient towards the exterior. This permits them to be more easily accessible to the surface of the protein compared to $DNA^{C3'endo}$·RNA hybrid duplex, wherein, the

Table 1
Major (*M*) and minor (*m*) groove widths in DNA·RNA hybrids and *iso*DNA·RNA chimer

Hybrid type[a]	*M* (Å)	*m* (Å)	Reference
$DNA^{C3'endo}$·RNA hybrid	6.3	10.8	[38]
$DNA^{O4'endo}$·RNA hybrid	8.1	9.9	Present work
*iso*DNA·RNA hybrid	8.2	9.1	Present work
*iso*B DNA duplex	14.0	4.5	[17]
B DNA duplex	11.7	5.7	[66]
A RNA duplex	4.2	11.1	[65]

[a] Eleven-fold hybrid duplex with helical parameter of $n=11$, $h=3$ Å and $t=32.7°$. 5.8 Å is subtracted from the P…P separation to account for the van der Waal's radii of the phosphate groups.

anionic oxygen atoms point into the mouth of major groove, thus making them less accessible to the protein surface. This, together with the increased intra-nucleotide P…P separation (6.7 Å), facilitates better interaction of the DNA strand with the enzyme (Table 2). As a result, Asn 16 (of the glycine-rich loop), Lys 99 (in the basic protrusion region), Gln 76, Gln 80, Trp 81 (which forms a kink between helices αII and αIII) are involved in hydrogen bonding with the anionic oxygen of the P_{10} and P_{12} phosphates of the $DNA^{O4'endo}$ backbone (Fig. 16). It is clear from Table 2 that these interactions are not conspicuous in the case of $DNA^{C3'endo}$·RNA hybrid. The interacting phosphates are located nearly at the center of the 19-mer hybrid duplex. Involvement of the

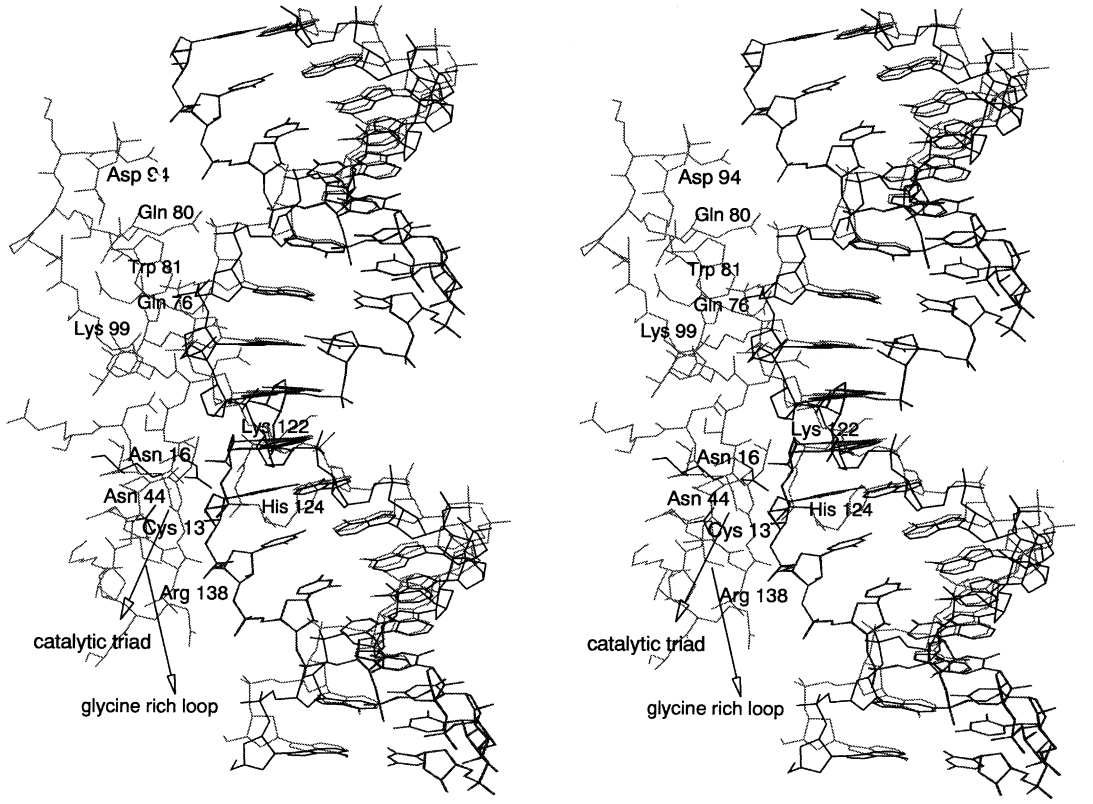

Fig. 15. Stereoplot of the interaction of $DNA^{(O4'endo)}$ (gray)·RNA (black) hybrid, and *iso*DNA (black)·RNA (black) with the *E. coli* RNase H. Only the portion of the protein involving the glycine rich loop, the basic protrusion region and other amino acid residues in the protein–DNA·RNA, (*iso*DNA/RNA) interface alone are shown for clarity. The residues and different regions of the protein chain involved in interaction with the DNA and RNA strand are indicated. Note the absence of interaction involving the *iso*DNA and RNase H as compared with the $DNA^{O4'endo}$ strand (see also Table 2).

Table 2
Comparison of interaction of DNA$^{(C3'endo)}$·RNA, DNA$^{(O4'endo)}$·RNA and *iso*DNA·RNA hybrid duplexes with *E. coli* RNase H

Interactions	DNA$^{C3'endo}$·RNA (Å)	DNA$^{O4'endo}$·RNA (Å)	*iso*DNA·RNA (Å)
Asp 94 (OD_1…O1P) (RNA) **P_1**	3.4	3.4	3.4
Gln 72 (NE_2…O_2') (RNA)	2.9	2.9	2.9
Gln 72 (NE_2…O_4') (RNA)	2.8	2.8	2.8
Lys 122 (NZ…O_1P) (RNA) **P_9**	3.4	3.4	3.4
Cys 13 (O…O_2') (RNA)	2.7	2.7	2.7
Cys 13 (O…O_3') (RNA)	3.0	3.0	3.0
Asn 44 (OG…O_2') (RNA)	2.9	2.9	2.9
Asn 44 (ND_2…O_2') (RNA)	3.3	3.3	3.3
Arg 138 (NH_2…O_2P) **P_1** (DNA)	5.5	5.0	6.4
Asn 16 (ND_2…O_1P) **P_9** (DNA)	5.9	3.4	3.9
Lys 99 (NZ…O_1P) **P_{10}** (DNA)	5.0	3.0	4.3
Gln 76 (NE_2…O_3') (DNA)	5.0	3.4	4.2
Gln 80 (NE_2…O_1P) **P_{12}** (DNA)	5.2	2.7	4.3
Trp 81 (NE_1…O_1P) **P_{12}** (DNA)	4.9	3.5	3.7

NE_2, NZ, ND_2 correspond to the amino group of the side chains. **P** corresponds to the phosphates of the DNA/RNA chain. Numbering of phosphates for the DNA (*iso*DNA) and RNA chain are from the 5′ side.

phosphate groups in the preferential interaction of *E. coli* RNase H with DNA·RNA hybrid has been suggested from enzyme–substrate affinity studies [74]. Our studies seem to provide a structural basis for these arguments.

Site directed mutagenesis [71] of Cys 13, Asn 16, Asn 44, Asn 45 and Gln 72 or His 124 by Ala is found to reduce the binding affinity of the substrate to *E. coli* RNase H. Also, replacement of Lys 122 by Asn and Arg 138 by Cys reduces the binding affinity to some extent. Reduction in binding affinity due to the mutation of Lys 122, Asn 16, Gln 72, Cys 13 and Asn 44 by Ala can be clearly interpreted as being due to loss of interactions (mostly hydrogen bonds) involving the side chain of these residues with the DNA or RNA backbone (see Table 2). On the other hand, interactions involving the residues Asn 45 with the RNA chain, as well as His 124 and Arg 138 with the DNA backbone are not clear as the distances of these residues from the hybrid duplex are greater than 5 Å. It is possible that the nature of their interactions may become clear when both the protein and the DNA·RNA hybrid are allowed to flex.

3.2.2. Interaction of isoDNA·RNA chimer with E. coli RNase H

As mentioned earlier a switch from 3′,5′ to 2′,5′ linkage is associated with a change in the sugar pucker preference [16,17,40] as well as a lateral shift of the sugar–phosphate backbone from the periphery towards the interior of the helix, which in turn, causes shrinkage of the minor groove width by approximately 1.7 Å (9.1 Å) in the *iso*DNA·RNA duplex. Interaction studies carried out similar to the above show that the prominent interactions involving Asn 16, Gln 76, Gln 80, Trp 81 and Lys 99 with the *iso*DNA backbone are totally lost (Fig. 15). As discussed above, all these interactions are found to be critical in the (DNA·RNA)×RNase H complex (Table 2). It may be remarked that although the *iso*DNA·RNA hybrid also has a groove width (9.1 Å) intermediate between A and B DNA duplexes, its structural features are quite different from that of the

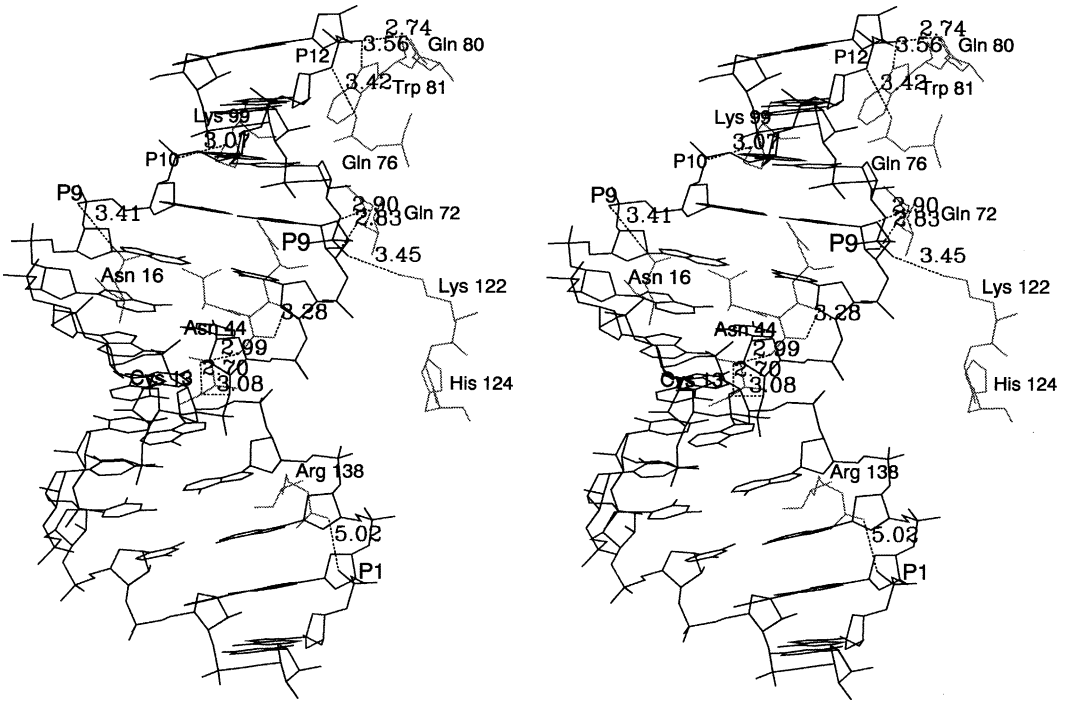

Fig. 16. Stereoplot showing the interaction involving the DNA$^{(O4'endo)}$ (black)·RNA (gray) hybrid with *E. coli* RNase H (see also Table 2).

DNA·RNA hybrid, and it is these geometrical and topological features that are responsible for the inhibitive action on *E. coli* RNase H.

4. Conclusions

The results from the present analysis have shown that change of linkage chemistry from 3′,5′ to 2′,5′ in nucleic acids brings forth stereochemical changes that have significant influence on the ability of formation of equivalent duplex and triplex structures known in nucleic acids with 3′,5′ linkages. They introduce conformational and topological constraints on the helical structures formed with 2′,5′ linkages and also contribute towards lowering their stability by reducing stacking interactions. NMR investigation on 2′,5′ RNA [40] and 2′,5′ DNA fragments [18] shows that they favor A type duplexes. These, along with the observations made from the present study that the formation of a 2′,5′ duplex or a triplex demands mandatory slide and displacement, the traits of the A-type duplex, argue in favor of A type duplexes dominating 2′,5′ nucleic acids. This is understandable, since this facilitates better interstrand base stacking interactions compared to the B-form (for *iso*DNA), which do not facilitate strong intrastrand stacking due to the mandatory requirements of slide and displacement. These indicate that 2′,5′ nucleic acids lack the ability for helical polymorphism. This is in sharp contrast to DNA, which is known to be highly flexible and capable of exhibiting high conformational polymorphism. Linkage change also imposes certain topological constraints in relation to groove dimensions. All of these, together with the fact that 2′,5′ links do not support the biologically relevant B form and the consequent related inadequacies, could have been the contributing factors towards their rejection. The structural changes caused by 2′,5′ linkages in the DNA chain clearly explains why it acts as an

inhibitor to *E. coli* RNase H when the *iso*DNA is complexed with RNA.

Acknowledgments

Authors thank DST for financial support. B.J. Premraj thanks CSIR for SRF. UGC is thanked for the grant to the department through the DSA.

References

[1] A. Eschenmoser, Chemical etiology of nucleic acid structures, Science 284 (1999) 2118–2124.
[2] M. Beier, F. Reck, T. Wagner, R. Krishnamurthy, A. Eschenmoser, Chemical etiology of nucleic acid structure: comparing pentopyranosyl-(2′–4′) oligonucleotides with RNA, Science 283 (1999) 699–703.
[3] M. Egholm, O. Buchardt, L. Christensen, et al., PNA hybridizes to complementary oligonucleotides obeying the Watson–Crick hydrogen bonding rules, Nature 365 (1993) 566–568.
[4] C. Hendrix, H. Rosemeyer, B. de Bouvere, A. van Aerschot, F. Seela, P. Herdewijn, 1′,5′-Anhydro hexitol oligonucleotides: hybridization and strand displacement with oligoribonucleotides, interaction with RNase H and HIV reverse transcriptase, Chem. Eur. J. 3 (1997) 1513–1520.
[5] E. Uhlmann, A. Peyman, Antisense oligonucleotides: a new therapeutic principle, Chem. Rev. 90 (1990) 543–584.
[6] A. De Mesmaeker, R. Hasner, P. Martin, E.H. Moser, Antisense oligonucleotides, Acc. Chem. Res. 28 (1995) 366–374.
[7] S.M. Frier, K.-H. Altmann, The ups and downs of nucleic acid duplex stability: structure-stability studies on chemically-modified DNA:RNA duplexes, Nucleic Acids Res. 25 (1997) 4429–4443.
[8] J. Wengel, Synthesis of 3′-C and 4′-C branched oligodeoxynucleotides and the development of locked nucleic acids (LNA), Acc. Chem. Res. 32 (1999) 301–310.
[9] M.M. Dhingra, R.H. Sarma, Why do nucleic acids have 3′,5′ phosphodiester bonds?, Nature 272 (1978) 798–801.
[10] R. Parthasarathy, M. Malik, S.M. Friday, X-Ray structure of a dinucleoside monophosphate A2′p5′C that contains a 2′–5′ link found in (2′,5′) oligo(A)s induced by interferons: single stranded helical conformation of 2′,5′ linked oligonucleotides, Proc. Natl. Acad. Sci. USA. 79 (1982) 7292–7296.
[11] R.H. Sarma, M.M. Dhingra, Evolution of nucleic acids conformation: the rational for the presence of 3′,5′ and the absence of 2′,5′ internucleotide linkage, in: R. Srinivasan, R.H. Sarma (Eds.), Conformation in Biology, Adenine Press, NY, 1982, pp. 259–265.
[12] J.P. Dougherty, C.J. Rizzo, R. Breslow, Oligodeoxynucleotides that contain 2′,5′ linkages: synthesis and hybridization properties, J. Am. Chem. Soc. 114 (1992) 6254–6255.
[13] H. Hashimoto, C. Switzer, Self association of 2′,5′ linked deoxynucleotides meta-DNA, J. Am. Chem. Soc. 114 (1992) 6255–6256.
[14] R. Kierzek, L. He, D.H. Turner, Association of 2′–5′ oligoribonucleotides, Nucleic Acids. Res. 20 (1992) 1685–1690.
[15] K.E. Jung, C. Switzer, 2′,5′ DNA containing guanine and cytosine forms stable duplexes, J. Am. Chem. Soc. 116 (1994) 6059–6061.
[16] V. Lalitha, N. Yathindra, Even nucleic acids with 2′,5′ linkages facilitate duplexes and structural polymorphism: prospects of 2′,5′-oligonucleotides as antigene/antisense tool in gene regulation, Curr. Sci. 68 (1995) 68–75.
[17] B.J. Premraj, N. Yathindra, Stereochemistry of 2′,5′ nucleic acids and their constituents, J. Biomol. Struct. Dyn. 16 (1998) 313–327.
[18] H. Robinson, K.-E. Jung, C. Switzer, A.H.-J. Wang, DNA with 2′,5′ phosphodiester bonds forms a duplex in the A-type conformation, J. Am. Chem. Soc. 117 (1995) 837–838.
[19] P.A. Giannaris, M.J. Damha, Oligonucleotides containing 2′,5′-phosphodiester linkages exhibit binding selectivity for 3′,5′-RNA over 3′,5′-ssDNA, Nucleic Acids Res. 21 (1993) 4742–4749.
[20] M. Wasner, D. Arion, G. Borkow, et al., Physicochemical and biophysical properties of 2′,5′-linked RNA and 2′,5′-RNA: 3′,5′-RNA 'hybrid' duplexes, Biochemistry 37 (1998) 7478–7486.
[21] R. Alul, G. Hoke, (2′-5′)-oligo-3′-deoxynucleotides: selective binding of single-stranded RNA but not DNA, Antisense Res. Develop. 5 (1995) 3–11.
[22] H. Sawai, J. Seki, H. Ozaki, Comparative studies of duplex and triplex formation of 2′-5′ and 3′-5′ linked oligoribonucleotides, J. Biomol. Struct. Dyn. 13 (1996) 1043–1051.
[23] T.P. Prakash, K-E. Jung, C. Switzer, RNA recognition by the 2′ structural isomer of DNA, J. Chem. Soc. Chem. Commun. (1996) 1793-1794.
[24] M.J. Darnha, A. Noronha, Recognition of nucleic acid double helices by homopyrimidine 2′,5′-linked RNA, Nucleic Acids Res. 26 (1998) 5152–5156.
[25] T.L. Sheppard, R.C. Breslow, Selective binding of RNA, but not DNA, by complementary 2′,5′-linked DNA, J. Am. Chem. Soc. 118 (1996) 9810–9811.
[26] P. Bhan, A. Bhan, M. Hong, J.G. Hartwell, J.M. Saunders, G.H. Hoke, 2′,5′-linked oligo-3′-deoxyribonucleoside phosphorothioate chimeras: thermal stability and antisense inhibition of gene expression, Nucleic Acids Res. 25 (1997) 3310–3317.
[27] E.R. Kandimalla, A. Manning, Q. Zhao, et al., Mixed backbone antisense oligonucleotides and biological properties of oligonucleotides containing 2′-5′-ribo- and

3′-5′-deoxyribonucleotide segments, Nucleic Acids Res. 25 (1997) 370–378.
[28] P.J.C. Smith, S. Arnott, LALS: Linked-atom least-squares reciprocal-space refinement system incorporating stereochemical restraints and supplement sparse diffraction data, Acta Cryst. A34 (1978) 3–11.
[29] S. Arnott, S.D. Dover, A.J. Wonacott, Least-squares refinement of the crystal and molecular structure of DNA and RNA from X-ray data and standard bond lengths and angles, Acta Cryst. B25 (1969) 2192–2206.
[30] S. Arnott, D.W.L. Hukins, Optimised parameters for A-DNA and B-DNA, Biochem. Biophys. Res. Commun. 47 (1972) 1504–1509.
[31] R. Chandrasekaran, S. Arnott, The structure of DNA and RNA helices in oriented fibers, Landolt–Bornstein Numerical Data and Functional Relationships in Science and Technology, vol. V11/1b, Springer Verlag, 1989, pp. 31–170.
[32] W.D. Cornell, P. Ciepek, C.I. Bayly, et al., A second generation force field for the simulation of protein, nucleic acids and organic molecules, J. Am. Chem. Soc. 117 (1995) 5179–5197.
[33] D.A. Pearlman, D.A. Case, J.W. Cadwell, et al., A package of computer programs for applying molecular mechanisms, normal mode analysis, molecular dynamics and free energy calculation to simulate the structure and energetic properties of molecules, Comp. Phys. Comm. 91 (1995) 1–41.
[34] U. Essmann, L. Perera, M.L. Berkowitz, T.A. Darden, H. Lee, L.G. Pederson, A smooth particle mesh Ewald method, J. Chem. Phys. 103 (1995) 8577–8593.
[35] T.E. Cheatham, P.A. Kollman, Observation of the A-DNA to B-DNA transition during unrestrained molecular dynamics in aqueous solution, J. Mol. Biol. 259 (1996) 434–444.
[36] G. Ravishankar, S. Swaminathan, D.L. Beveridge, R. Lavery, H.J. Sklenar, Conformational and helicoidal analysis of 30ps of molecular dynamics in d(CGCGAATTCGCG) double helix: 'Curves' dials and windows, J. Biomol. Struct. Dyn. 6 (1989) 669–699.
[37] R. Lavery, H. Sklenar, The definition of generalized helicoidal parameters and of axis curvature for irregular nucleic acids, J. Biomol. Struct. Dyn. 6 (1988) 63–91.
[38] S. Arnott, R. Chandrasekkaran, R.P. Millane, H.S. Park, DNA–RNA hybrid secondary structures, J. Mol. Biol. 188 (1986) 631–640.
[39] Biosym Inc. Insight II. Biosym, Inc., San Diego, CA, USA (1993).
[40] B.J. Premraj, P.K. Patel, E.R. Kandimalla, S. Agrawal, R.V. Hosur, N. Yathindra, NMR structure of a 2′,5′ RNA favours an A type duplex with compact C2′*endo* nucleotide repeat, Biochem. Biophys. Res. Commun 283 (2001) 537–543.
[41] N. Yathindra, M. Sundaralingam, Analysis of the possible helical structures of nucleic acids and polynucleotides. Application of (n–h) plots, Nucleic Acids Res. 3 (1976) 729–747.
[42] W.K. Olson, The spatial configuration of ordered polynucleotide chains. I. Helix formation and base stacking, Biopolymers 15 (1976) 859–878.
[43] R. Malathi, N. Yathindra, Backbone conformation in nucleic acids: an analysis of the local helicity through heminucleotide scheme and a proposal for the unified conformation plot, J. Biomol. Struct. Dyn. 3 (1985) 127–144.
[44] L. Trantirek, R. Stefl, M. Vorlickova, J. Koca, V. Sklenar, J. Kypr, An A-type double helix of DNA having B-type puckering of the deoxyribose rings, J. Mol. Biol. 297 (2000) 907–922.
[45] B. Schneider, H.M. Berman, Hydration of DNA bases is local, Biophys. J. 69 (1995) 2661–2669.
[46] B. Schneider, K. Patel, H.M. Berman, Hydration of phosphate group in double helical DNA, Biophys. J. 75 (1998) 2422–2434.
[47] G. Felsenfeld, D.R. Davies, A. Rich, Formation of a three-stranded polynucleotide molecule, J. Am. Chem. Soc. 79 (1957) 2023–2024.
[48] C. Helene, The antisense strategy: control of gene expression by triplex forming oligonucleotides, Anticancer Drug Design 6 (1991) 569–584.
[49] E. Postel, S.J. Flint, D.J. Kessler, M.E. Hogan, Evidence that a triplex-forming oligodeoxyribonucleotide binds to the C-myc promoter in HeLa cells, thereby reducing C-cyc mRNA levels, Proc. Natl. Acad. Sci. USA 88 (1991) 8227–8231.
[50] G. Raghunathan, H.T. Miles, V. Sasisekharan, Symmetry and molecular structure of a DNA triple helix: $d(T)_n \cdot d(A)_n \cdot d(T)_n$, Biochemistry 32 (1993) 455–462.
[51] F.B. Howard, J. Frazier, M.N. Lipsett, H.T. Miles, Infrared demonstration of two- and three-strand helix formation between poly C and guanosine mononucleotides and oligonucleotides, Biochem. Biophys. Res. Commun. 17 (1964) 93–97.
[52] J. Liquier, P. Coffinier, M. Frion, E. Taillandier, Triple helical polynucleotidic structures: sugar conformations determined by FTIR spectroscopy, J. Biomol. Struct. Dyn. 9 (1991) 437–445.
[53] C.Y. Sekharadu, N. Yathindra, M. Sundaralingam, Molecular dynamics investigations of DNA triple helical models: unique features of the Watson–Crick duplex, J. Biomol. Struct. Dyn. 11 (1993) 225–243.
[54] R. Jin, W.H. Chapman, A.R. Srinivasan, W.K. Olson, R. Breslow, K.J. Breslauer, Comparative spectroscopic, calorimetric and computational studies of nucleic acid complexes with 2′,5′- versus 3,5′-phosphodiester linkages, Proc. Nad. Acad. Sci. USA 90 (1993) 10568–10572.
[55] A.R. Srinivasan, W.K. Olson, Molecular models of nucleic acid triple helixes. II. PNA and 2′,5′ backbone complexes, J. Am. Chem. Soc. 120 (1998) 492–499.
[56] S.B. Zimmerman, B.H. Pheiffer, An RNA.DNA hybrid that can adopt two conformation: an X-ray diffraction

study of poly(dA)·poly(dT) in concentrated solution or fibers, Proc. Nat. Acad. Sci. USA 78 (1981) 78–82.
[57] G. Milman, R. Langridge, M.J. Chamberlin, The structure of a DNA–RNA hybrid, Proc. Nat. Acad. Sci. USA 57 (1967) 1804–1810.
[58] S.H. Chou, P. Flyn, B.R. Reid, High resolution NMR study of a synthetic DNA/RNA hybrid dodecamer containing the consensus Pribnow promoter sequence d(CGTTATAATGCG): r(CGCAUUAUAACG), Biochemistry 28 (1989) 2435–2443.
[59] G.L. Conn, T. Brown, G.A. Leonard, The crystal structure of the RNA/DNA hybrid r(GAAGAGAAGC)·d(GCTTCTCTTC) shows significant differences to that found in solution, Nucleic Acids Res. 27 (1999) 555–561.
[60] M. Katahira, S.J. Lee, Y. Kobayashi, et al., Structure in solution of the RNA/DNA hybrid $(rA)_8$:$(dT)_8$ determined by NMR and Raman spectroscopy, J. Am. Chem. Soc. 112 (1990) 4508–4512.
[61] H. Shindo, U. Matsumotu, Direct evidence for a bimorphic structure of a DNA/RNA hybrid, poly(rA):poly(dT), at high relative humidity, J. Biol. Chem. 259 (1984) 8682–8684.
[62] A.H.-J. Wang, S. Fuji, J.H. van Boom, G.A. van der Marel, S.A.A. van Boeckel, A. Rich, Molecular structure of r(GCG) d(TATACGC): a DNA–RNA hybrid helix joined to double helical DNA, Nature 299 (1982) 601–604.
[63] Y. Xiong, M. Sundaralingam, Crystal structure of a DNA·RNA hybrid duplex with a polypurine RNA r(gaagaagag) and a complementary polypyrimidine DNA d(CTCTTCTTC), Nucleic Acids Res. 28 (2000) 2171–2176.
[64] Y. Fedoroff, M. Salazar, B.R. Reid, Structure of a DNA:RNA hybrid duplex. Why RNase H does not cleave pure RNA?, J. Mol. Biol. 233 (1993) 509–523.
[65] S. Arnott, D.W.L. Hukins, S.D. Dover, W. Fuller, A.R. Hodgson, Structures of synthetic polynucleotides in the A-RNA and A′-RNA conformations: X-ray diffraction analyses of the molecular conformations of polyadenylic acid·polyuridylic acid and polyinosinic acid·polycytidylic acid, J. Mol. Biol. 81 (1973) 107–122.
[66] S. Arnott, D.W.L. Hukins, Optimised parameters for A-DNA and B-DNA, Biochem. Biophy. Res. Commun. 47 (1972) 1504–1510.
[67] K. Katayanagi, M. Miagawa, M. Matsushima, et al., Three dimensional structure of ribonuclease H from *E. coli*, Nature 347 (1990) 306–309.
[68] K. Katayanagi, M. Miagawa, M. Matsushima, et al., Structural details of ribonuclease H from *Escherichia coli* as refined to an atomic resolution, J. Mol. Biol. 223 (1992) 1029–1052.
[69] W. Yang, W.A. Hendrickson, R.J. Crouch, Y. Satow, Structure of ribonuclease H phased at 2 Å resolution by MAD analysis of the selenomethionyl protein, Science 249 (1990) 1398–1405.
[70] W.G. Scott, J.T. Finch, A. Klug, The crystal structure of an all-RNA hammerhead ribozyme: a proposed mechanism for RNA catalytic cleavage, Cell 81 (1995) 991–1002.
[71] H. Nakamura, Y. Oda, S. Iwai, et al., How does RNase H recognise a DNA:RNA hybrid, Proc. Natl. Acad. Sci USA. 88 (1991) 11535–11539.
[72] G. Minasov, M. Teplova, P. Nielsen, J. Wengel, M. Egli, Structural basis of cleavage by RNase H of hybrids of arabinonucleic acids and RNA, Biochemistry 39 (2000) 3525–3532.
[73] M.J. Damha, C.J. Wilds, A. Noronha, et al., Hybrids of RNA and arabinonucleic acids (ANA and 2′F-ANA) are substrates of ribonuclease H, J. Am. Chem. Soc. 120 (1998) 12976–12977.
[74] W.F. Lima, S.T. Crooke, Binding affinity and specificity of *Escherichia coli* RNase HI: impact on the kinetics of catalysis of antisense oligonucleotide–RNA hybrids, Biochemistry 36 (1997) 390–398.